Supporting Information

Multifunctions of carbon dots in CeO_2/Cu_2O complex catalyst for the regulation of carbon dioxide reduction

Xiong Yan[a], Jiacheng Li[a], Honglin Si[a], Haojie Xu[a], Hui Huang[a]*,Yang Liu[a]*, Zhenhui Kang[a,b]*

[a] Institute of Functional Nano & Soft Materials (FUNSOM), Jiangsu Key Laboratory for Carbon-Based Functional Materials & Devices, Soochow University, 199 Ren'ai Road, Suzhou, 215123, Jiangsu, China.

[b] Macao Institute of Materials Science and Engineering (MIMSE), MUST-SUDA Joint Research Center for Advanced Functional Materials, Macau University of Science and Technology, Taipa 999078, Macao, China.

Supplementary Text

1. Materials

Cerium nitrate hexahydrate ($Ce(NO_3)_3 \cdot 6H_2O$, 99.5%) was purchased from Macklin. Nafion (~5%) was purchased from UTEPO Technology Suzhou Co. Copper(ii) nitrate hydrate ($Cu(NO_3)_2 \cdot 3H_2O$, AR) was purchased from Sinopharm. Sodium hydroxide (NaOH, 98%) and potassium bicarbonate ($KHCO_3$, 99.7%) were purchased from Aladdin. Graphite rod (99.99 %) was purchased from Alfa Aesar Co. Ltd. Ultrapure water (resistivity: $\rho \geq 18$ MΩ·cm) was used throughout the synthesis process.

2. Synthesis of CeO_2, Ce-Cu and Ce-Cu-CDs-x (x is the mass ratio of added CDs)

A hydrothermal method was used to synthesize CeO_2. Typically, 0.744 g of $Ce(NO_3)_3 \cdot 6H_2O$ and 9.6 g of NaOH were mixed and dissolved in 40 mL of deionized water. The mixed solution was ultrasonicated for an additional 30 min at room temperature and then the ink was transferred into a 100 mL Teflon reactor. The Teflon reactor was tightly sealed and subjected to hydrothermal treatment in an oven at 77 ℃ for 24 h. After cooling down to room temperature, the white precipitate obtained was collected, washed with ultrapure water and ethanol three times, and dried overnight in a vacuum oven at 80 ℃. The yellow powder obtained after drying was calcined in a muffle furnace at 450 ℃ for 3 h to get CeO_2.

CeO_2 was then used as precursor to prepare Ce-Cu. In order to prepare Ce-Cu, 0.1 g CeO_2 was ultrasonically dispersed in 20 mL deionized water, and 14.1 mg $Cu(NO_3)_2 \cdot 3H_2O$ was added. After stirring for 20 min, 0.5 mol/L Na_2CO_3 was added to adjust the pH to 9-10 of the solution. The mixed solution was centrifuged at 8000 rpm for 5 min, then it was dried overnight. The obtained powder was calcined in a muffle furnace at 500 ℃ for 3 h.

Ce-Cu was used to prepare the Ce-Cu-CDs-x. In order to prepare Ce-Cu-CDs-2.5 %, 0.1 g Ce-Cu was ultrasonically dispersed in 40 mL deionized water, and 2.5 mg CDs

were added. The mixed solution was stirred at 1500 rpm for 5 h and then vacuum dried to obtain the sample. Ce-Cu-CDs-0.5 %, Ce-Cu-CDs-1.25 %, Ce-Cu-CDs-3.75 %, Ce-Cu-CDs-5 %, and Ce-Cu-CDs-7.5 % were prepared in the same way, instead of that the amount of CDs added is 0.05 mg, 1.25 mg, 3.75 mg, 5 mg, and 7.5 mg.

3. Synthesis of CDs

CDs were prepared using graphite rod as carbon source by electrolysis method [1]. DC power supply with a fixed voltage of 30 V was used, and pure water was used as the electrolyte for electrolysis. After 20 days of electrolysis, the black solution was collected and filtered to remove the large carbon particles. Finally, the black solution was freeze-dried to obtain CDs.

4. Electrochemical measurements

All the electrochemical experiments were performed in a three-electrode system in a H-cell at room temperature. The platinum sheet was used as the counter electrode, the saturated calomel electrode (SCE) was used as the reference electrode, and the working electrode was carbon paper coated with catalyst (1 cm × 1.5 cm). 5 mg of catalyst was dispersed in 1000 μL 0.5 wt.% Nafion water solution to form a homogeneous ink after at least 10 min of ultrasonication. Then 400 μL of the catalyst ink was dropped on the two sides of carbon fiber paper and dried at 70 ℃ to get the working electrode. The CO_2RR performance experiment was carried out by constant potential electrolysis in the H-cell. 6 μL catalyst dispersion solution was dropped on the glassy carbon electrode, and dried at room temperature. Linear sweep voltammetry (LSV) curves were performed from 0 V to -1.7 V *vs.* SCE in N_2-saturated and CO_2-saturated 0.5 M $KHCO_3$ solution, respectively. N_2 and CO_2 needed were continuously ventilated for at least 20 min to ensure that the solution was completely saturated. All the potentials were converted to RHE, according to the equation E (*vs.* RHE) = E (*vs.* SCE) + 0.059 × pH + 0.241.

5. Product analysis

For the product analysis, the measurements were performed in an airtight electrochemical H-type cell with two chambers separated by a slice of proton exchange membrane (Nafion 212). The cathode chamber included a working electrode and a reference electrode, while the anode compartment was composed of a platinum wire as the counter electrode. Each of the chambers was loaded with 35.0 mL 0.5 M $KHCO_3$ (saturated with CO_2) and 30.0 mL of CO_2 in the headspace. To activate the catalyst, 50 cycles of CV from 0 V to -1.8 V (*vs.* SCE) were performed prior to potentiostatic electrocatalysis. After applying a constant voltage to the working electrode for a specific duration, the gas in the cathode chamber was extracted using a disposable syringe for further analysis. Pana A60 gas chromatograph was employed to detect and analyze carbon containing gas products (CO, CH_4, C_2H_4 and C_2H_6). H_2 was detected and determined by gas chromatograph with east-west analysis. The liquid product was analyzed by nuclear magnetic resonance (NMR, Bruker AVANCEAV III 400) spectrometer. 500 μL of electrolyte after reaction, 100 μL D_2O and 0.05 μL dimethyl sulfoxide (DMSO, Sigma, 99.99%) were mixed as the internal standard. The FE of various products was calculated by the following formula:

$$FE = \frac{znF}{Q} \times 100\%$$

where z is the number of electrons transferred, F is the faraday constant (96485 $C \cdot mol^{-1}$), and n is the number of moles of the produced products.

6. Computational details

Spin-polarized electronic structure calculations were performed using the plane-wave basis set approach as implemented in the Vienna ab initio simulation package (VASP) [2]. The projector augmented wave (PAW) method was used to represent the ion–core electron interactions [3]. The valence electrons were represented with a plane wave basis set with an energy cutoff of 450 eV. Electronic exchange and correlation were described with the Perdew–Burke–Ernzerhof (PBE) functional [4]. DFT-D3 method was used to treat the van der Waals interaction [5]. A 2×2×1 Monkhorst–Pack scheme was used to

generate the k-point grid for the modeled surfaces [6]. The convergence criteria for the self-consistent electronic structure and geometry were set to 10^{-5} eV and 0.05 eV/Å, respectively.

7. Transient photovoltage (TPV) measurements

The TPV responses were conducted on a home-made measurement system. The excitation source is a laser radiation pulse from a third harmonic Nd: YAG laser (Beamtech Optronics Co., Ltd, wavelength of 355 nm and the repetition rate is 5 Hz). The TPV signal was registered by a 5 GHz digital oscilloscope (MDO3104, Tektronix). The signal of the TPV was first amplified and then recorded by an oscilloscope. All measurements were performed at room temperature and ambient pressure. TPV measurements were carried out using a platinum mesh (1 cm × 1 cm) covering the sample as the working electrode and a platinum wire as the electrode at room temperature.

Supplementary Figures

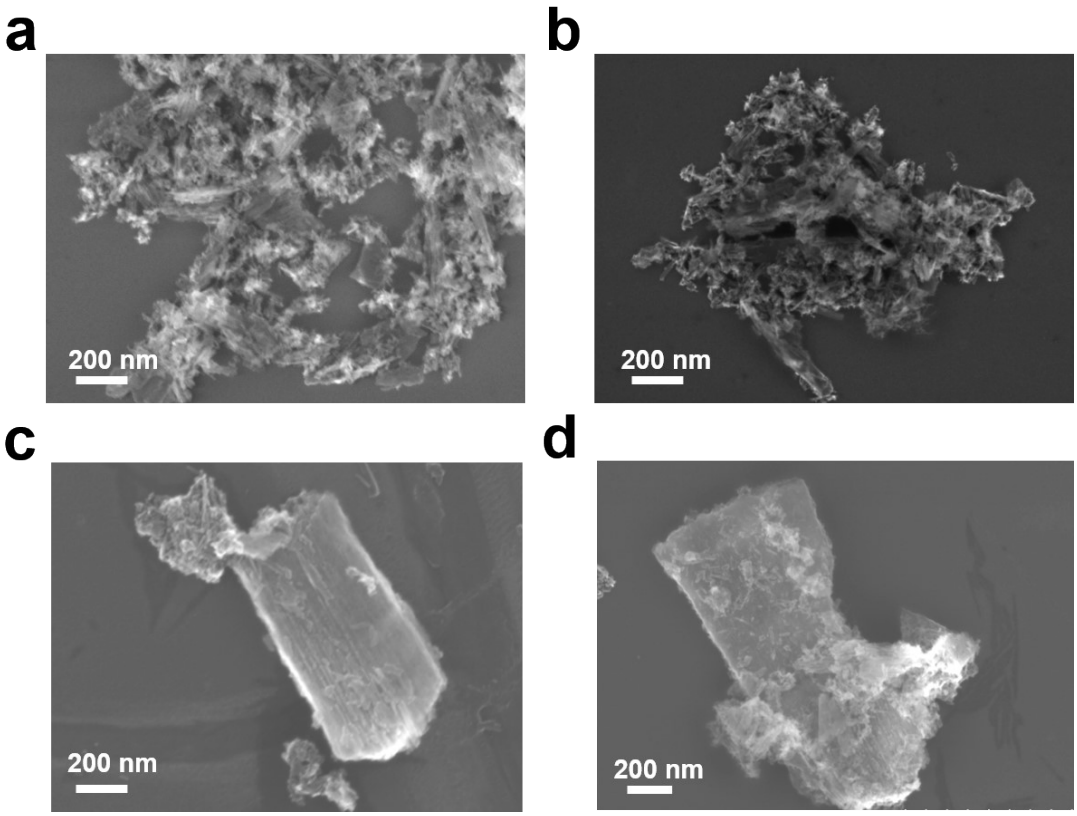

Figure S1. SEM images of (a) Ce-Cu, (b) CeO_2, (c) Ce-Cu-CDs-2.5% and (d) Ce-Cu-CDs-5%.

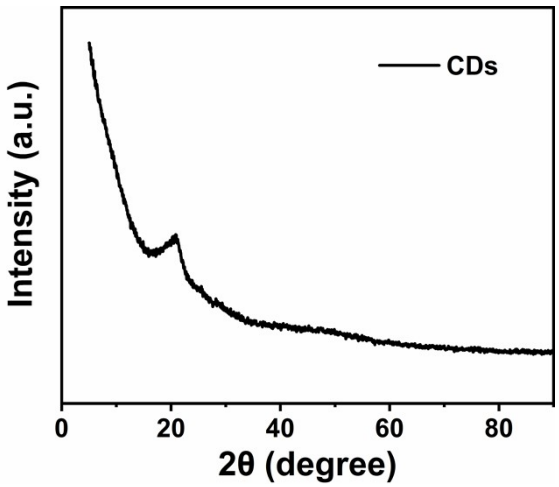

Figure S2. The XRD pattern of CDs.

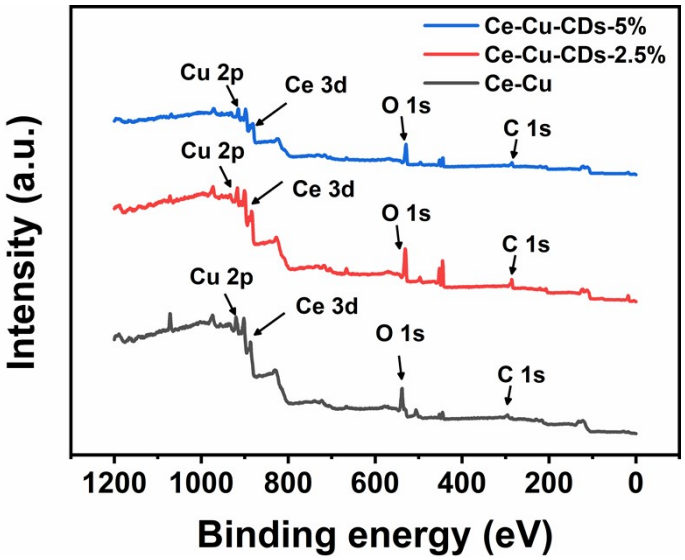

Figure S3. The full survey XPS spectra of Ce-Cu, Ce-Cu-CDs-2.5% and Ce-Cu-CDs-5%.

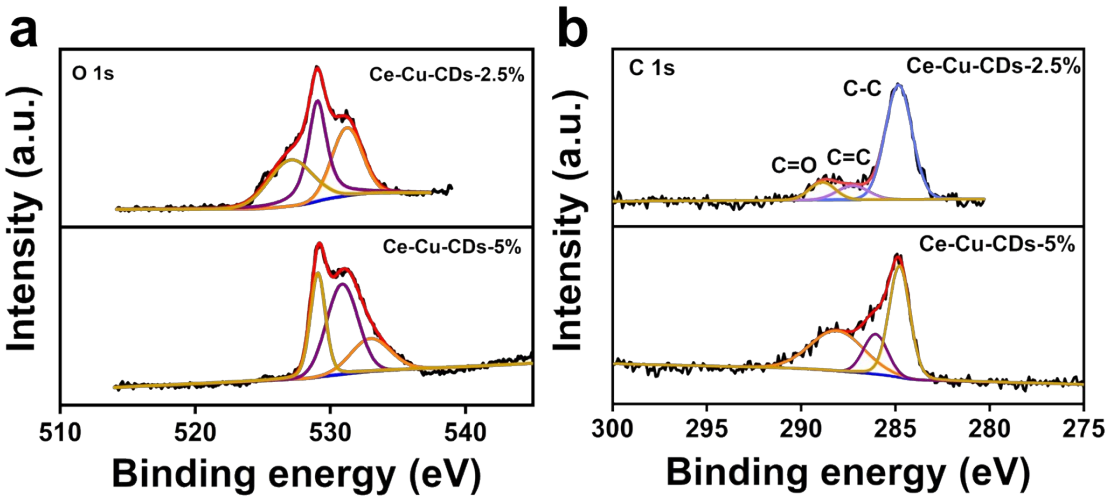

Figure S4. (a) High-resolution XPS spcetra of O 1s for Ce-Cu-CDs-2.5% and Ce-Cu-CDs-5%. (b) High-resolution XPS spcetra of C 1s for Ce-Cu-CDs-2.5% and Ce-Cu-CDs-5%.

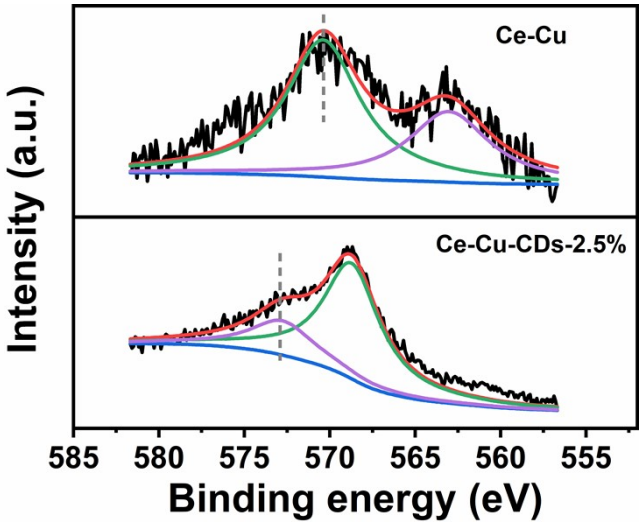

Figure S5. Cu LMM spectra for Ce-Cu and Ce-Cu-CDs-2.5%

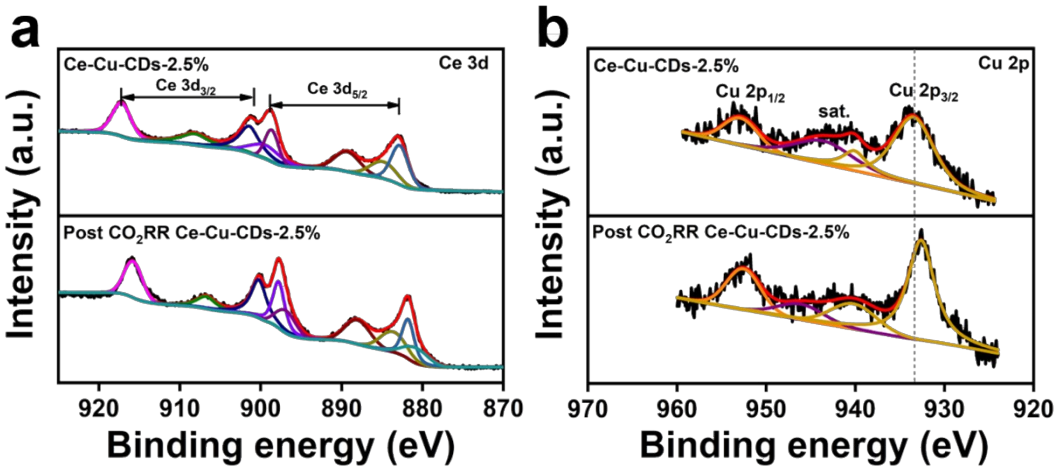

Figure S6. (a) XPS spectra of Ce 3d with Ce-Cu-CDs-2.5% and Post CO_2RR Ce-Cu-CDs-2.5%. (b) XPS spectra of Cu 2p with Ce-Cu-CDs-2.5% and Post CO_2RR Ce-Cu-CDs-2.5%.

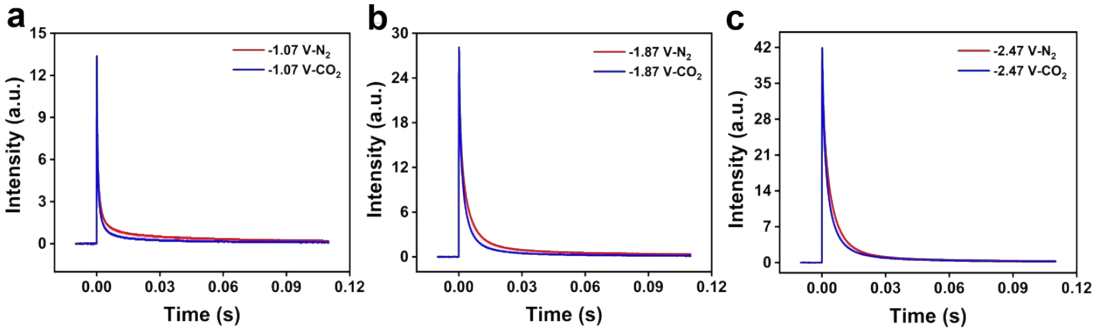

Figure S7. Current decay curves of CeO_2 in 0.5 M $KHCO_3$ saturated with CO_2/N_2 at (a) -1.07 V, (b) -1.87 V, and (c) -2.47 V *vs.* Hg/Hg_2Cl_2.

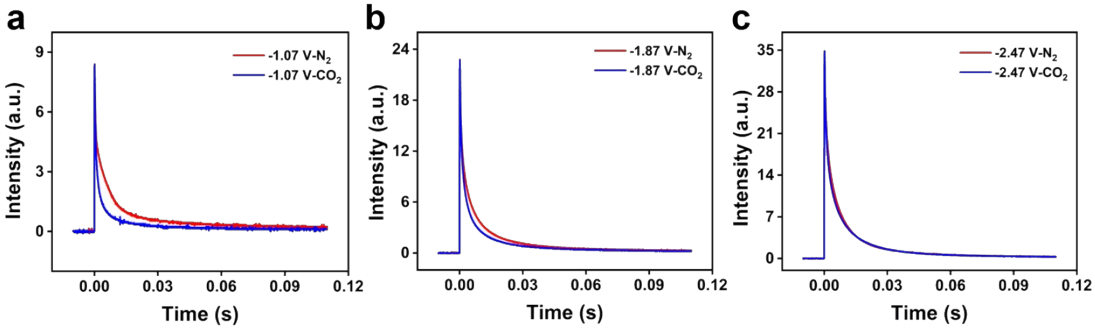

Figure S8. Current decay curves of Ce-Cu in 0.5 M $KHCO_3$ saturated with CO_2/N_2 at (a) -1.07 V, (b) -1.87 V, and (c) -2.47 V *vs.* Hg/Hg_2Cl_2.

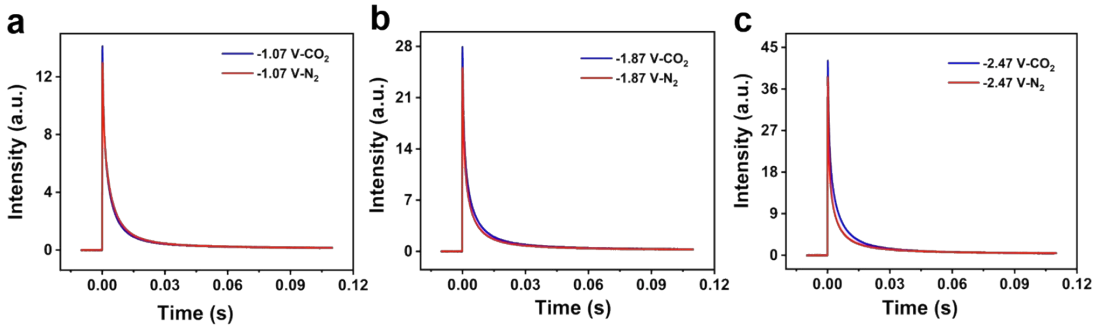

Figure S9. Current decay curves of Ce-Cu-CDs-0.5% in 0.5 M $KHCO_3$ saturated with CO_2/N_2 at (a) -1.07 V, (b) -1.87 V, and (c) -2.47 V *vs.* Hg/Hg_2Cl_2.

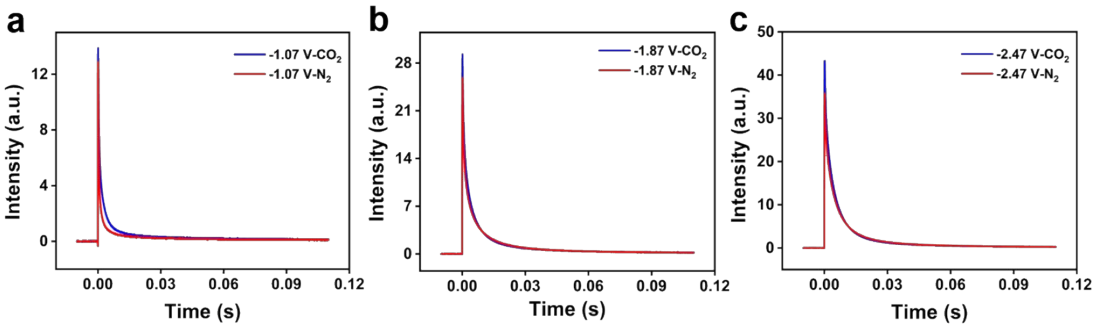

Figure S10. Current decay curves of Ce-Cu-CDs-1.25% in 0.5 M $KHCO_3$ saturated with CO_2/N_2 at (a) -1.07 V, (b) -1.87 V, and (c) -2.47 V *vs.* Hg/Hg_2Cl_2.

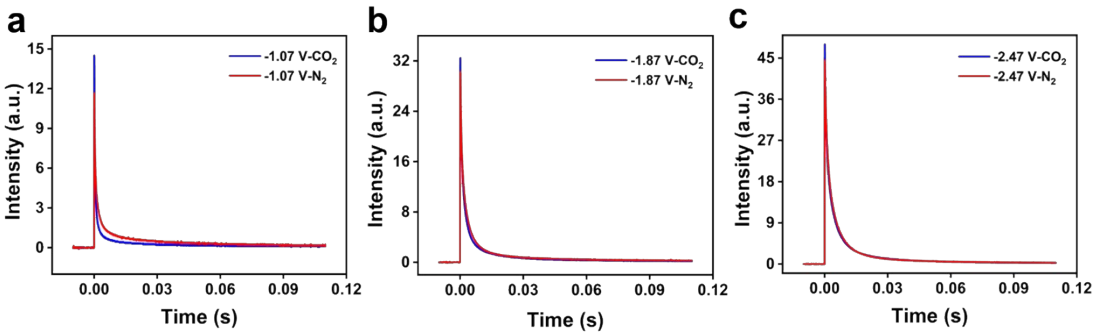

Figure S11. Current decay curves of Ce-Cu-CDs-2.5% in 0.5 M $KHCO_3$ saturated with CO_2/N_2 at (a) -1.07 V, (b) -1.87 V, and (c) -2.47 V *vs.* Hg/Hg_2Cl_2.

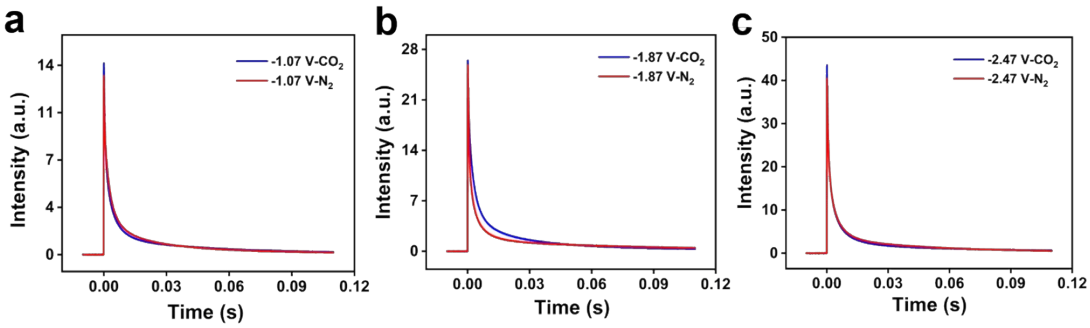

Figure S12. Current decay curves of Ce-Cu-CDs-3.75% in 0.5 M $KHCO_3$ saturated with CO_2/N_2 at (a) -1.07 V, (b) -1.87 V, and (c) -2.47 V *vs.* Hg/Hg_2Cl_2.

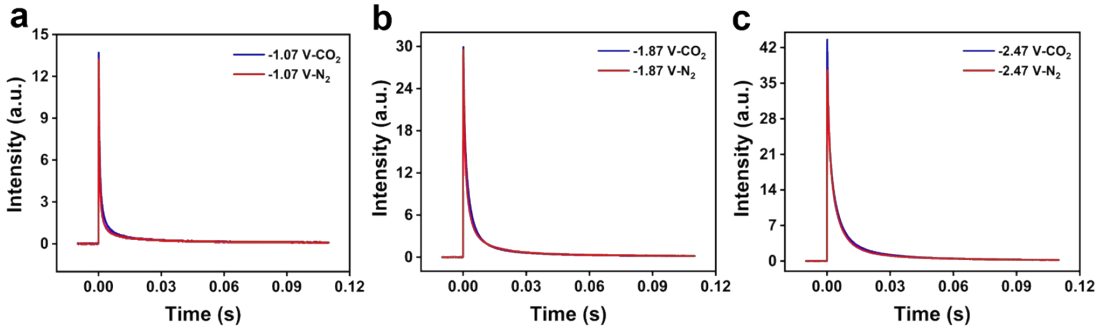

Figure S13. Current decay curves of Ce-Cu-CDs-5% in 0.5 M $KHCO_3$ saturated with CO_2/N_2 at (a) -1.07 V, (b) -1.87 V, and (c) -2.47 V *vs.* Hg/Hg_2Cl_2.

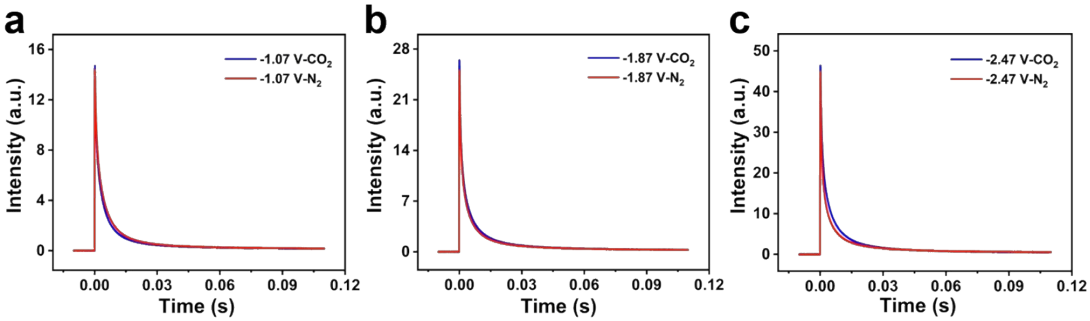

Figure S14. Current decay curves of Ce-Cu-CDs-7.5% in 0.5 M $KHCO_3$ saturated with CO_2/N_2 at (a) -1.07 V, (b) -1.87 V, and (c) -2.47 V *vs.* Hg/Hg_2Cl_2.

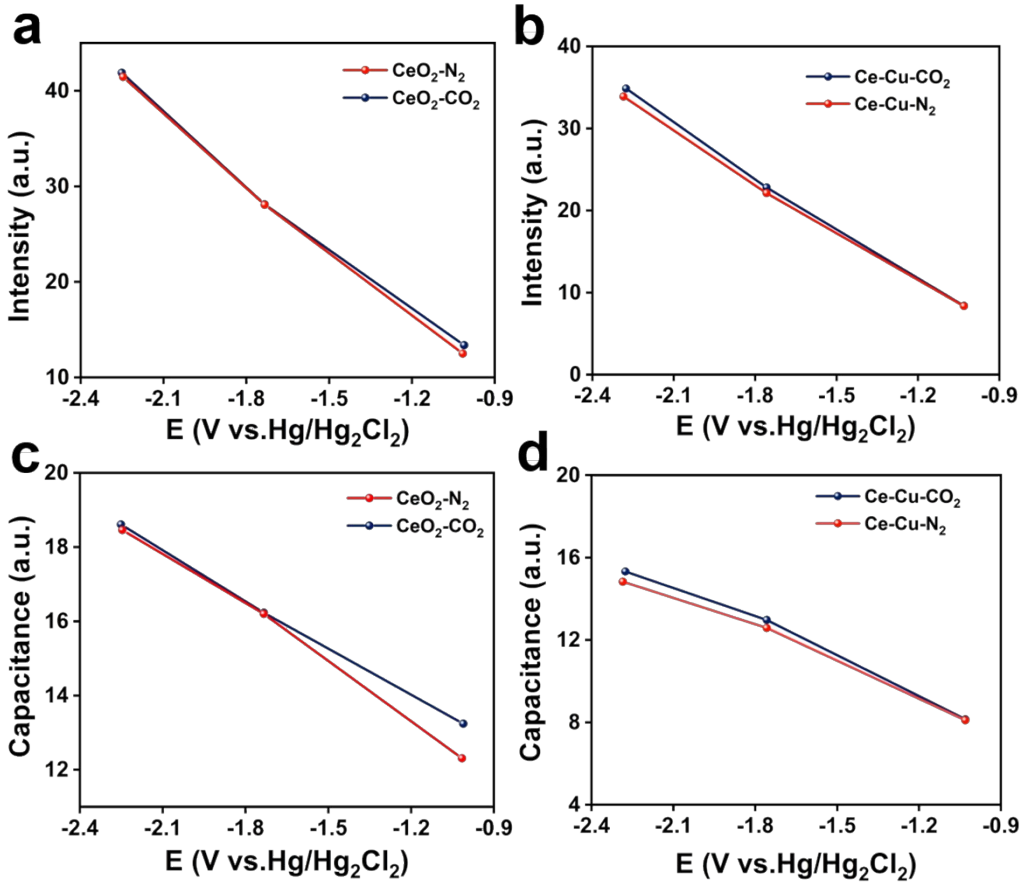

Figure S15. (a) C-U curves of CeO_2 obtained by TPS testing under different atmospheres. (b) I_{max}-U curves of CeO_2 obtained by TPS testing under different atmospheres. (c) C-U curves of Ce-Cu obtained by TPS testing under different atmospheres. (d) I_{max}-U curves of Ce-Cu obtained by TPS testing under different atmospheres

.

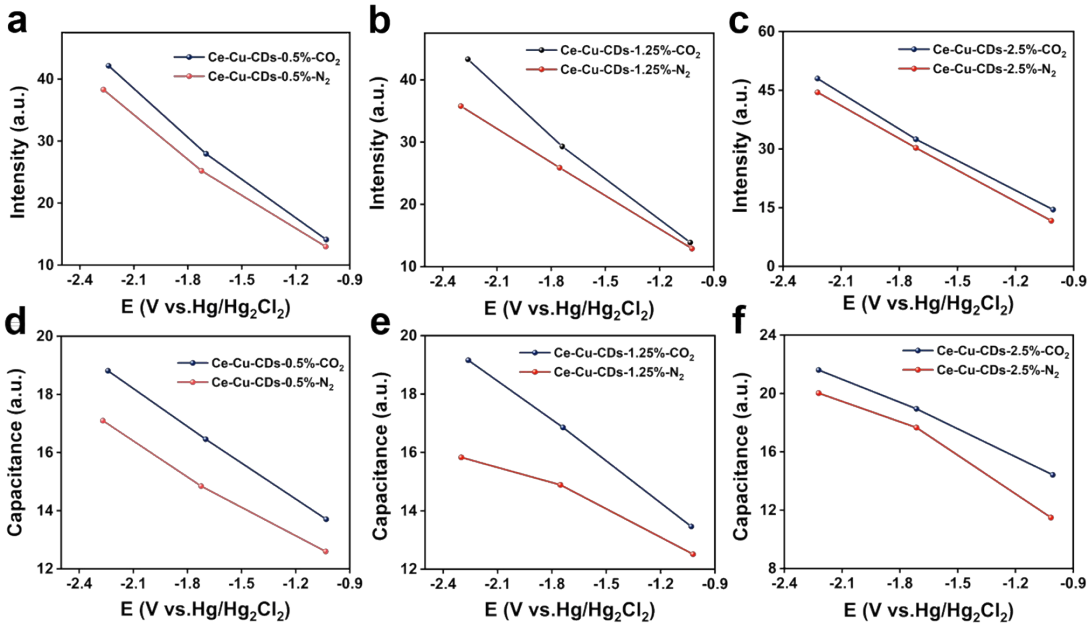

Figure S16. (a-c) I_{max}-U curves of Ce-Cu-CDs-0.5%, Ce-Cu-CDs-1.25% and Ce-Cu-CDs-2.5% obtained by TPS testing under different atmospheres, respectively. (d-f) C-U curves of Ce-Cu-CDs-0.5%, Ce-Cu-CDs-1.25% and Ce-Cu-CDs-2.5% obtained by TPS testing under different atmospheres, respectively.

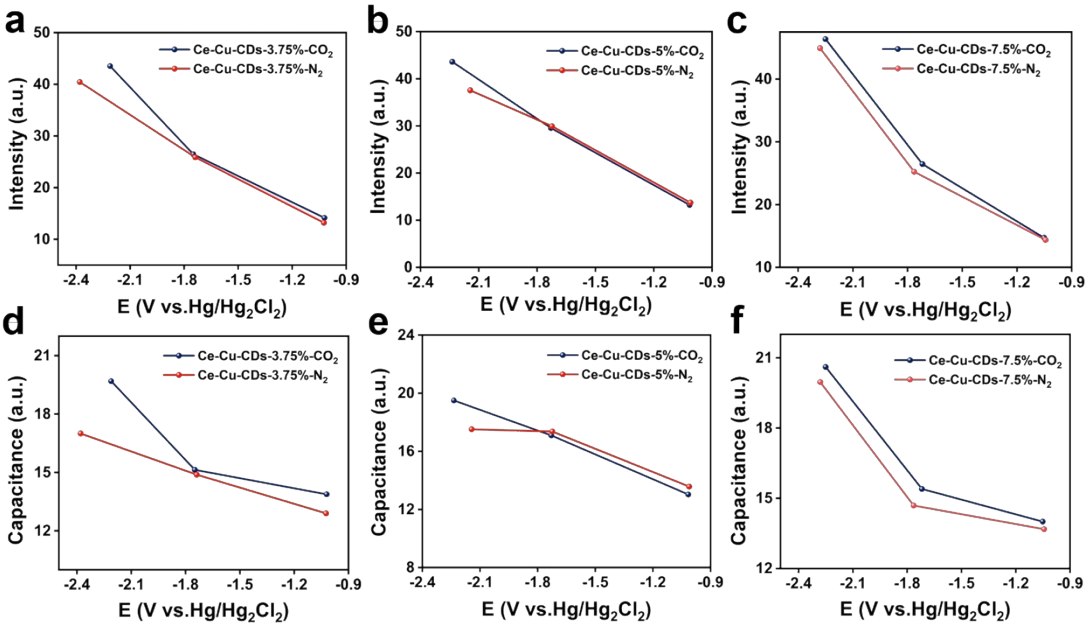

Figure S17. (a-c) I_{max}-U curves of Ce-Cu-CDs-3.75%, Ce-Cu-CDs-5% and Ce-Cu-CDs-7.5% obtained by TPS testing under different atmospheres, respectively. (d-f) C-U curves of Ce-Cu-CDs-3.75%, Ce-Cu-CDs-5% and Ce-Cu-CDs-7.5% obtained by TPS testing under different atmospheres, respectively.

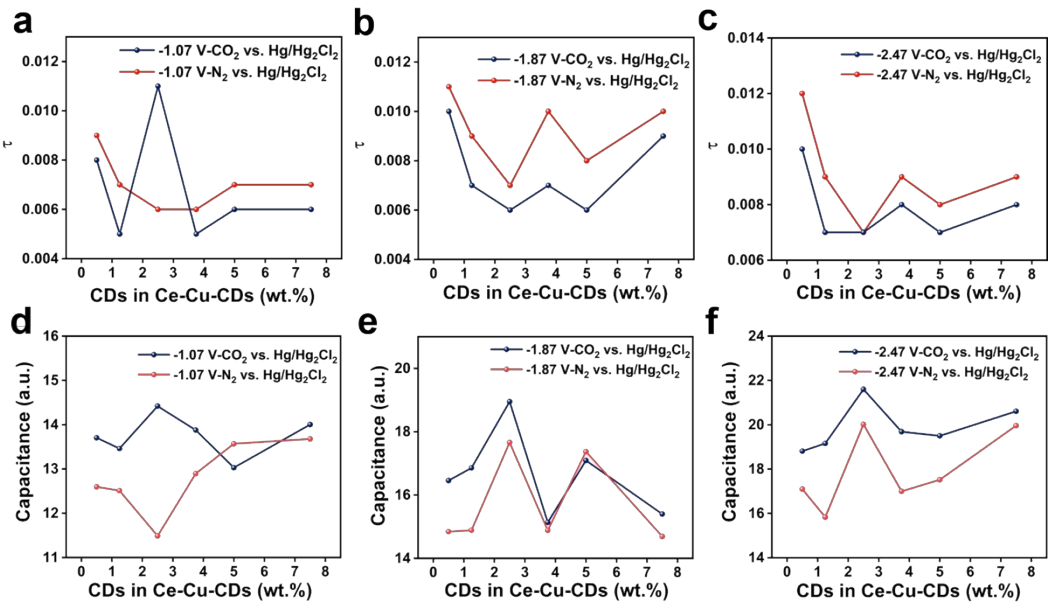

Figure S18. (a) The change of τ with different CDs concentrations at the same potential (-1.07 V *vs.* Hg/Hg_2Cl_2). (b) The change of τ at different CDs concentrations at the same potential (-1.87 V *vs.* Hg/Hg_2Cl_2). (c) The change of τ at different CDs concentrations at the same potential (-2.47 V *vs.* Hg/Hg_2Cl_2). (d) The change of capacitance at different CDs concentrations at the same potential (-1.07 V *vs.* Hg/Hg_2Cl_2). (e) The change of capacitance at different CDs concentrations at the same potential (-1.87 V *vs.* Hg/Hg_2Cl_2). (f) The change of capacitance at different CDs concentrations at the same potential (-2.47 V *vs.* Hg/Hg_2Cl_2).

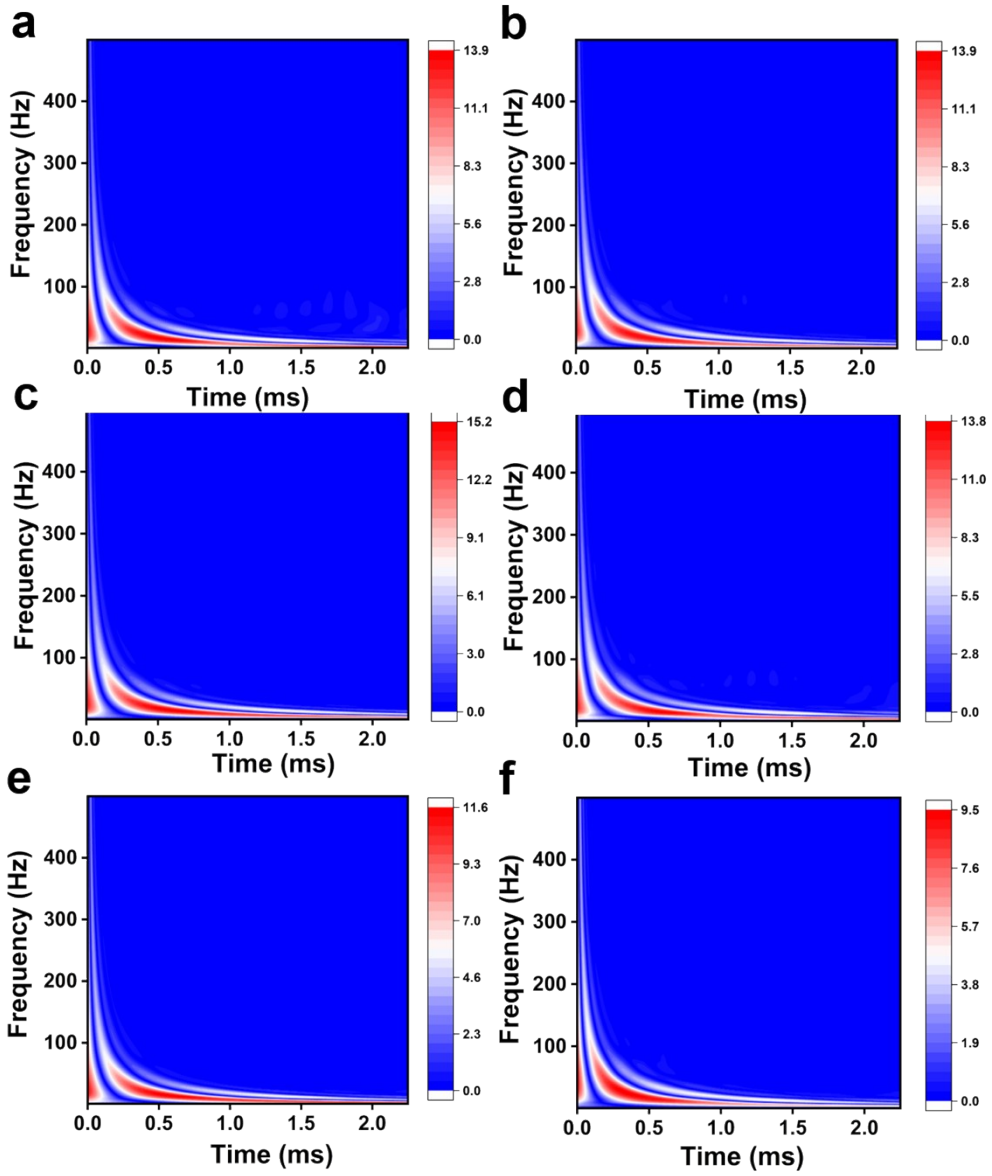

Figure S19. (a) CWT patterns of Ce-Cu-CDs-0.5% in CO_2 atmosphere. (b) CWT patterns of Ce-Cu-CDs-0.5% in N_2 atmosphere. (c) CWT patterns of Ce-Cu-CDs-1.25% in CO_2 atmosphere. (d) CWT patterns of Ce-Cu-CDs-1.25% in N_2 atmosphere. (e) CWT patterns of Ce-Cu-CDs-2.5% in CO_2 atmosphere. (f) CWT patterns of Ce-Cu-CDs-2.5% in N_2 atmosphere.

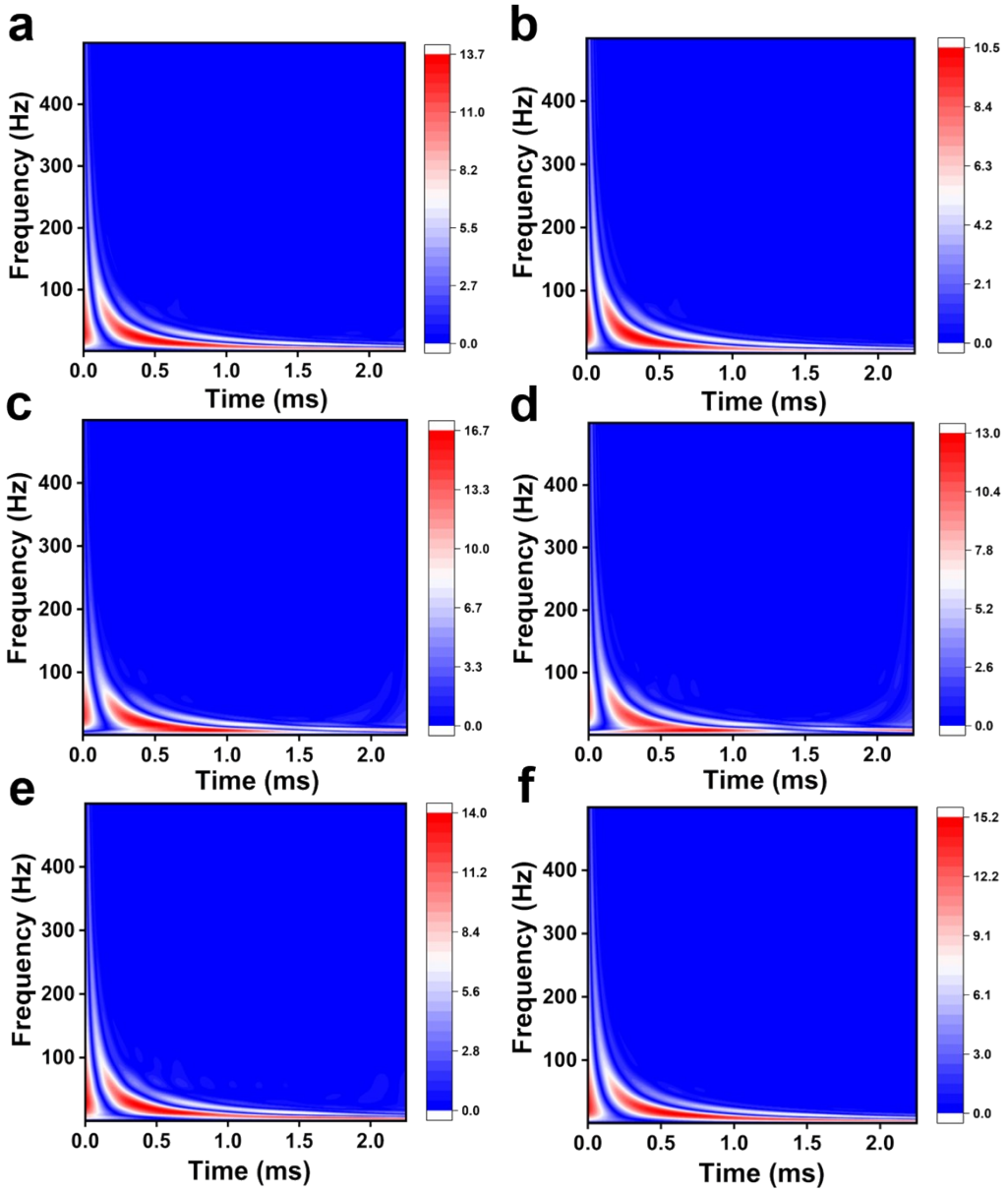

Figure S20. (a) CWT patterns of Ce-Cu-CDs-3.75% in CO_2 atmosphere. (b) CWT patterns of Ce-Cu-CDs-3.75% in N_2 atmosphere. (c) CWT patterns of Ce-Cu-CDs-5% in CO_2 atmosphere. (d) CWT patterns of Ce-Cu-CDs-5% in N_2 atmosphere. (e) CWT patterns of Ce-Cu-CDs-7.5% in CO_2 atmosphere. (f) CWT patterns of Ce-Cu-CDs-7.5% in N_2 atmosphere.

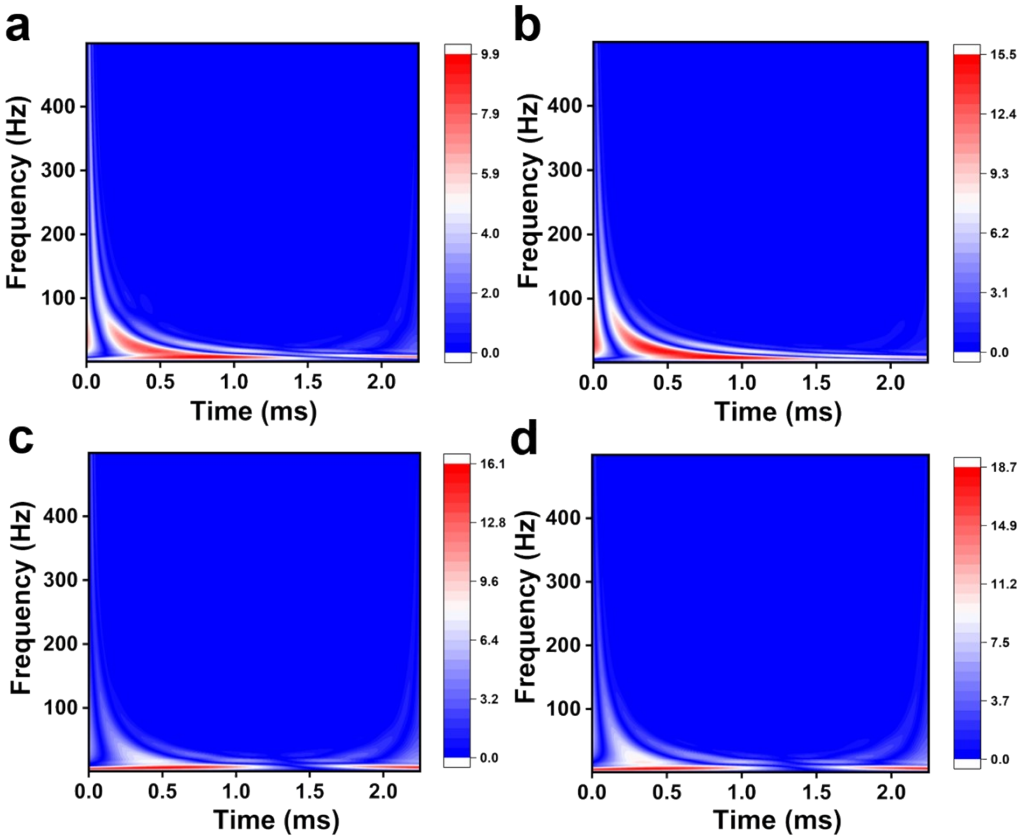

Figure S21. (a) CWT patterns of Ce-Cu in CO_2 atmosphere. (b) CWT patterns of Ce-Cu in N_2 atmosphere. (c) CWT patterns of CeO_2 in CO_2 atmosphere. (d) CWT patterns of CeO_2 in N_2 atmosphere.

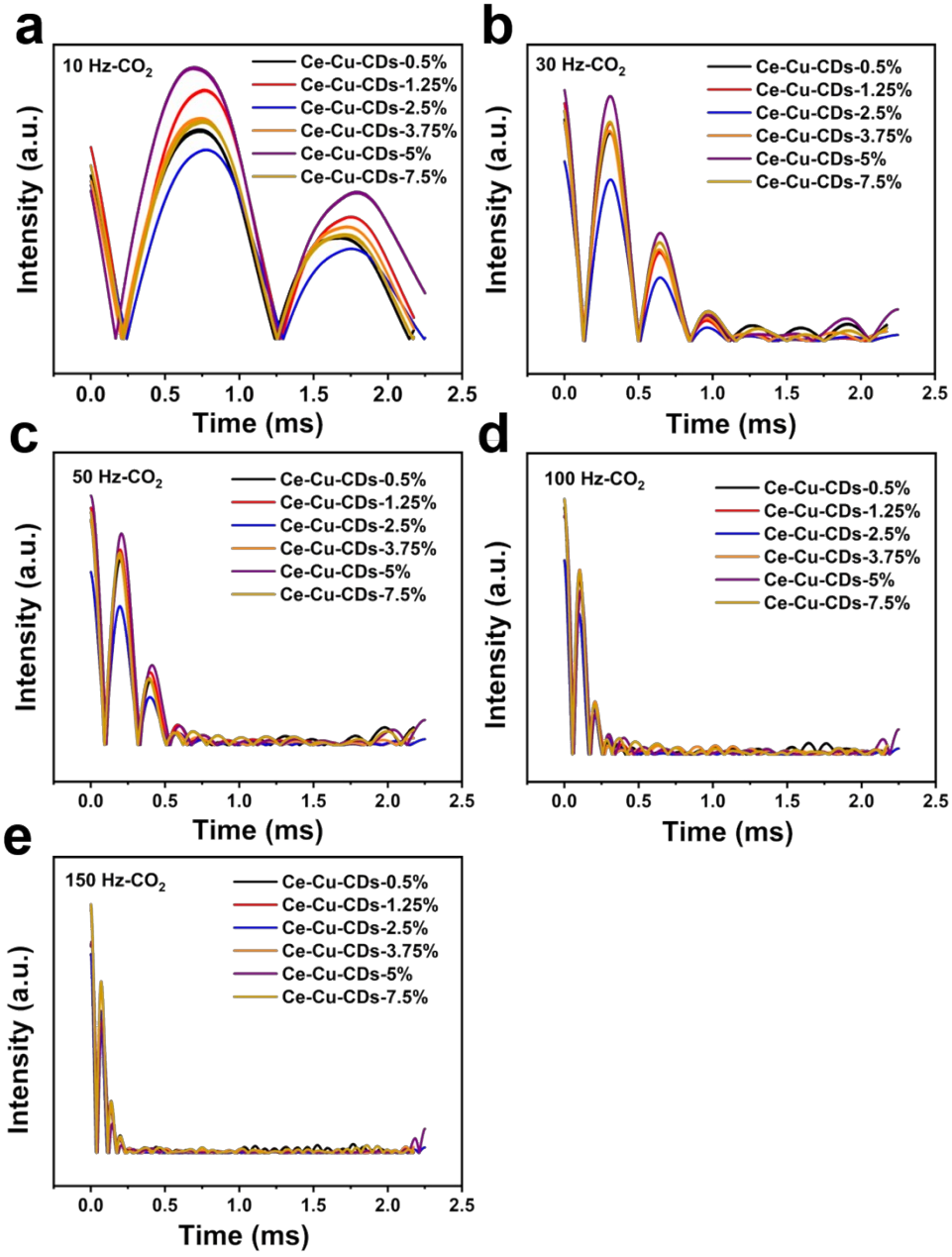

Figure S22. (a-e) Intensity-Time curves with the different frequency (10 Hz, 30 Hz, 50 Hz, 100 Hz and 150 Hz) of Ce-Cu-CDs-0.5%, Ce-Cu-CDs-1.25%, Ce-Cu-CDs-2.5%, Ce-Cu-CDs-3.75%, Ce-Cu-CDs-5%, and Ce-Cu-CDs-7.5% in CO_2 atmosphere.

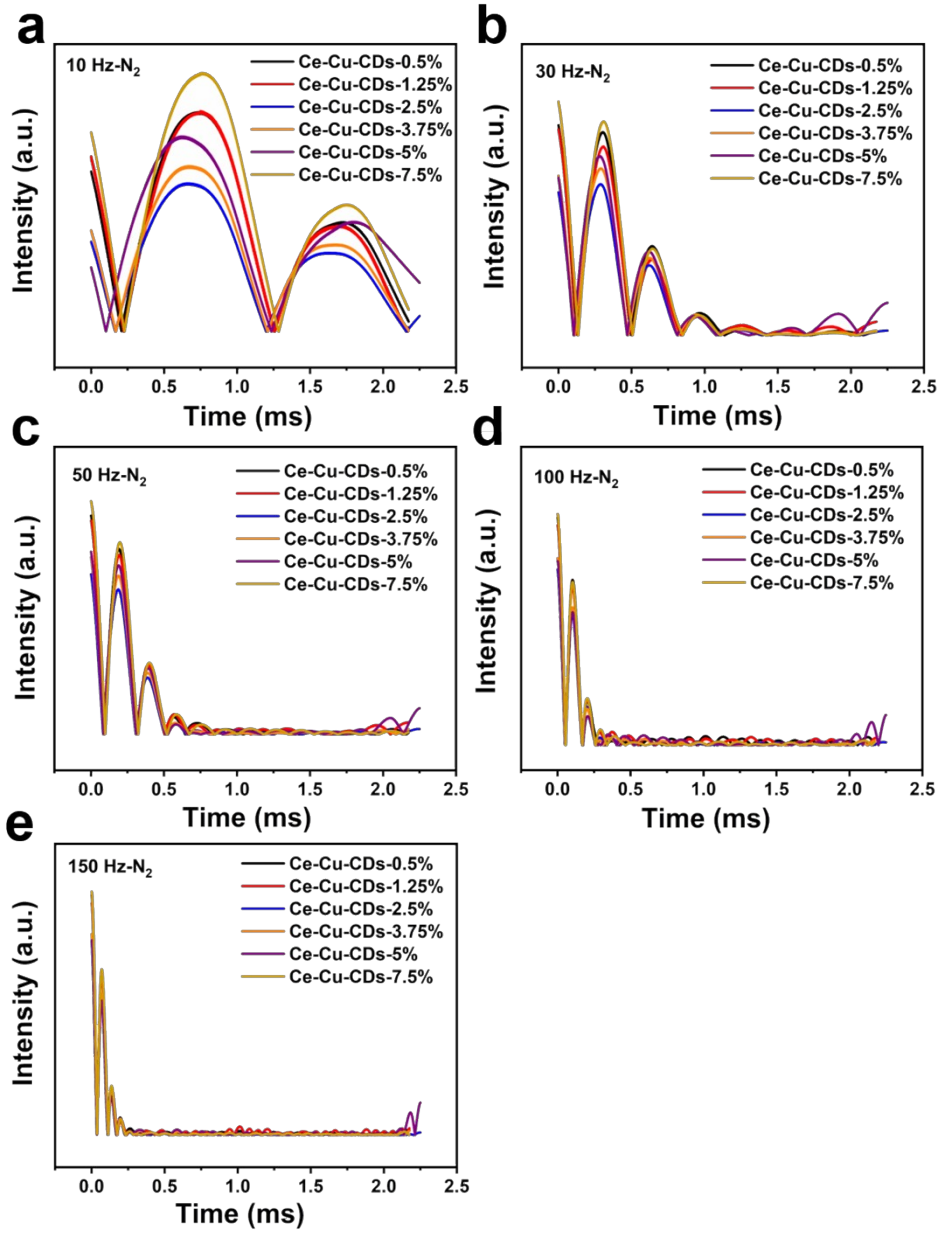

Figure S23. (a-e) Intensity-Time curve with the different frequency (10 Hz, 30 Hz, 50 Hz, 100 Hz and 150 Hz) of Ce-Cu-CDs-0.5%, Ce-Cu-CDs-1.25%, Ce-Cu-CDs-2.5%, Ce-Cu-CDs-3.75%, Ce-Cu-CDs-5%, and Ce-Cu-CDs-7.5% in N_2 atmosphere.

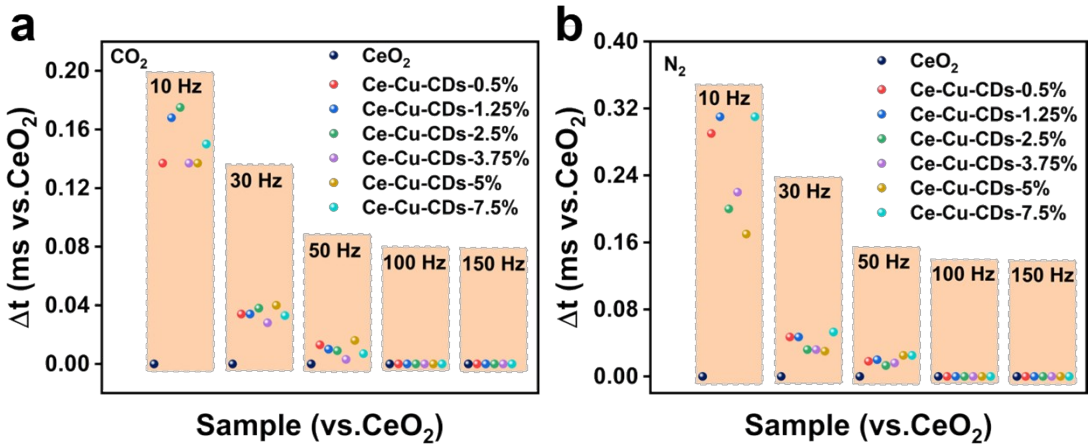

Figure S24. (a) The different frequencies deviation curves of CeO_2, Ce-Cu-CDs-0.5%, Ce-Cu-CDs-1.25%, Ce-Cu-CDs-2.5%, Ce-Cu-CDs-3.75%, Ce-Cu-CDs-5%, and Ce-Cu-CDs-7.5% in CO_2 atmospheres. (b) The different frequencies deviation curves of CeO_2, Ce-Cu-CDs-0.5%, Ce-Cu-CDs-1.25%, Ce-Cu-CDs-2.5%, Ce-Cu-CDs-3.75%, Ce-Cu-CDs-5%, and Ce-Cu-CDs-7.5% in N_2 atmospheres.

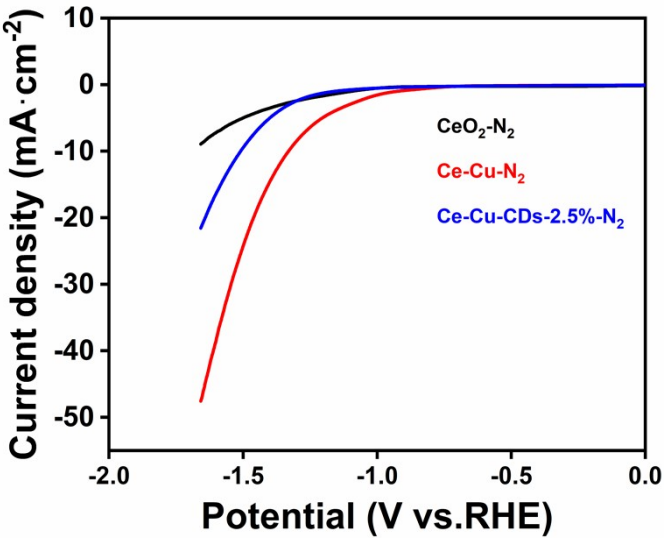

Figure S25. LSV curves of CeO_2, Ce-Cu and Ce-Cu-CDs-2.5% obtained in N_2-saturated 0.5 M $KHCO_3$ aqueous solution with a scanning rate of 50 $mV \cdot s^{-1}$.

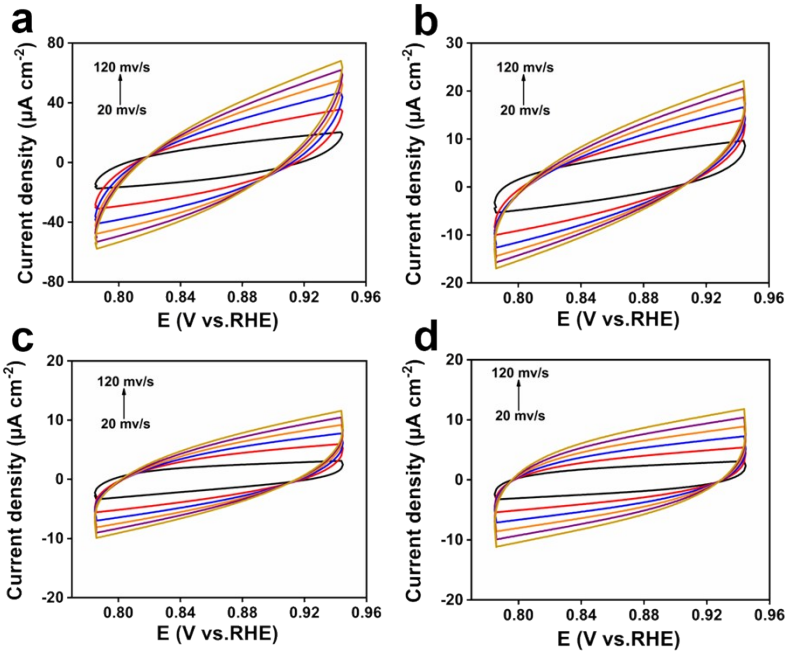

Figure S26. CV curves within the non-Faradic region of (a) CeO_2, (b) Ce-Cu, (c) Ce-Cu-CDs-2.5%, and (d) Ce-Cu-CDs-5% at the scan rates of 20, 40, 60, 80,100, and 120 $mV \cdot s^{-1}$, respectively.

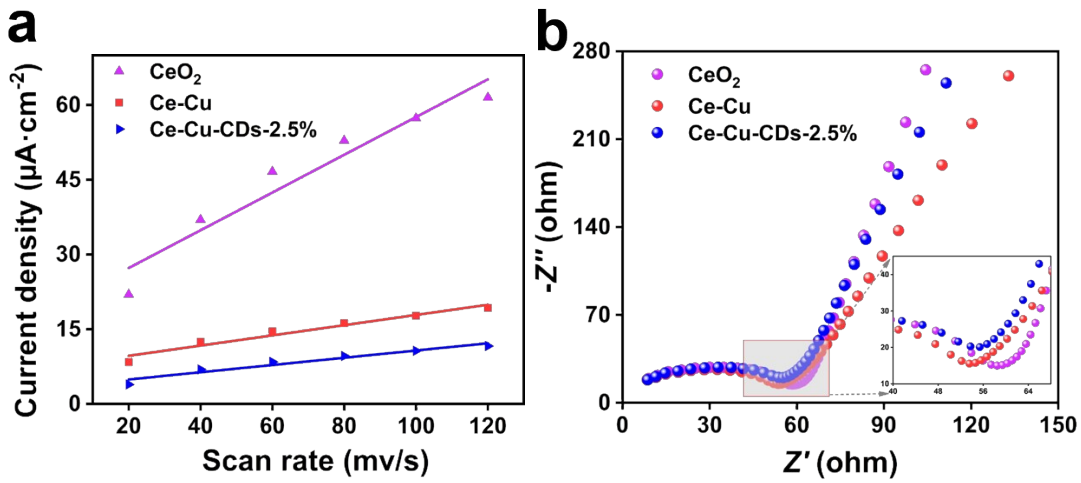

Figure S27. (a) C_{dl} recorded at the scan rates of 20, 40, 60, 80, 100, and 120 $mV \cdot s^{-1}$, respectively. (b) Comparison of potential-dependent Nyquist plots for CeO_2, Ce-Cu and Ce-Cu-CDs-2.5% measured in CO_2-saturated 0.5 M $KHCO_3$ aqueous solution.

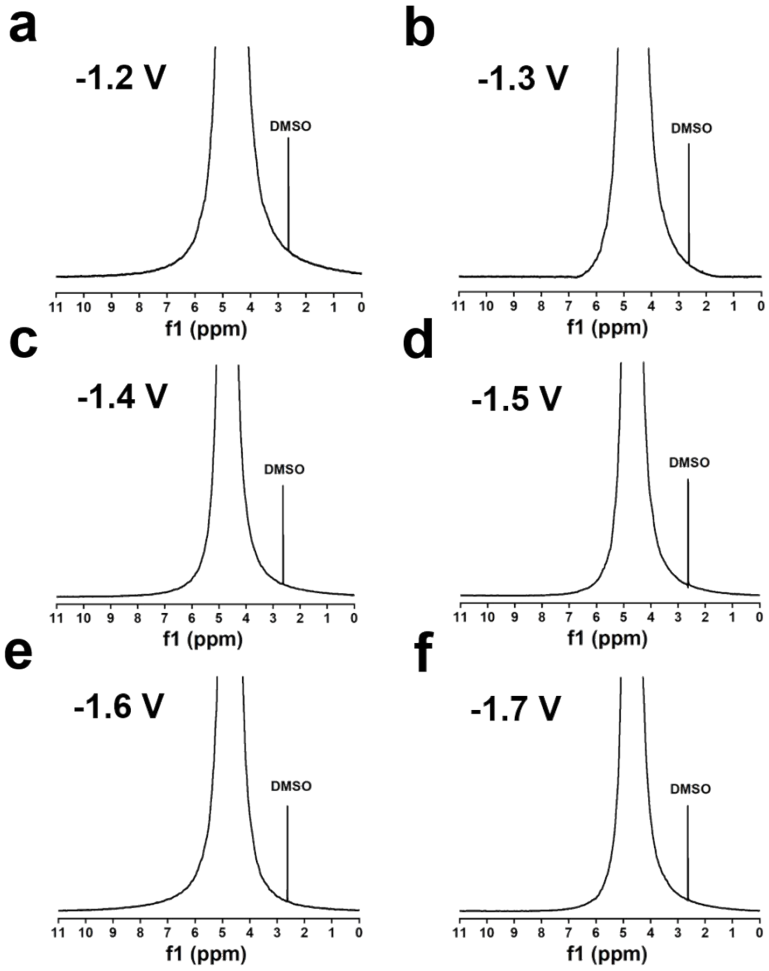

Figure S28. ^{1}H-NMR spectra of Ce-Cu in –1.2 ~ –1.7 V (*vs.* RHE).

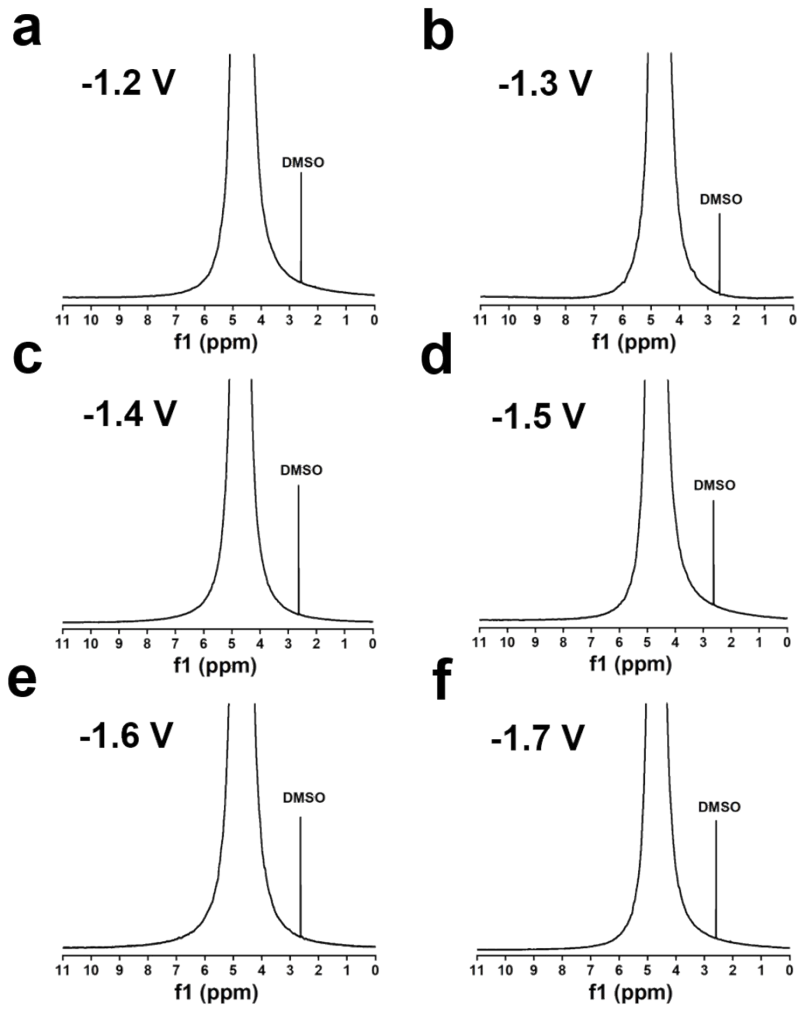

Figure S29. ^{1}H-NMR spectra of Ce-Cu-CDs-2.5% in –1.2~–1.7 V (*vs.* RHE).

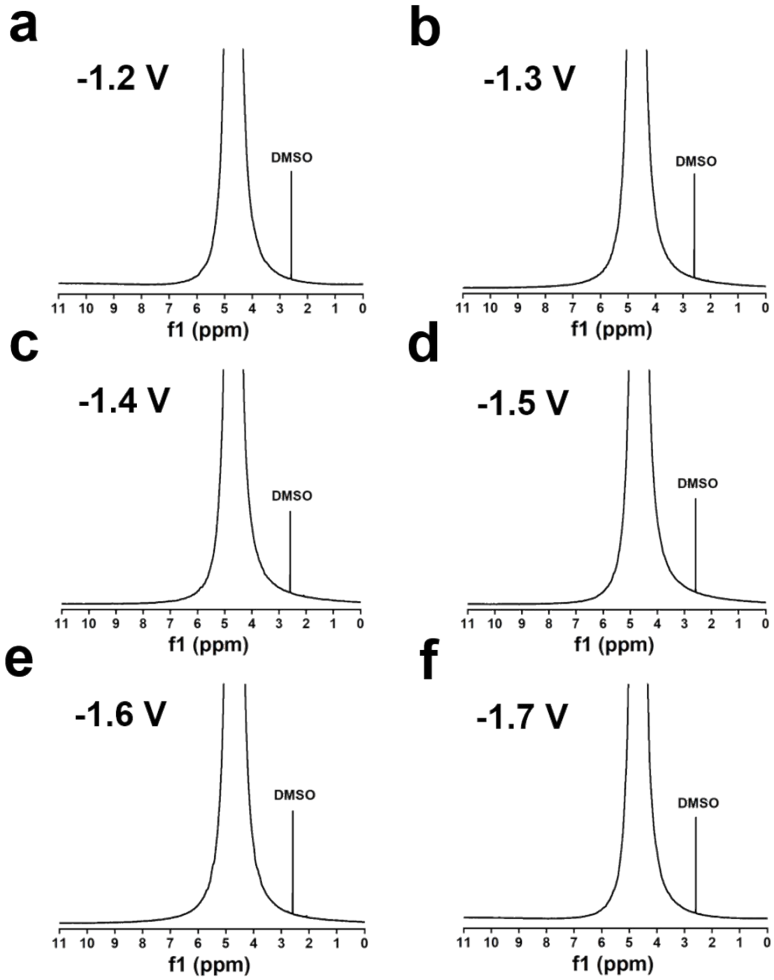

Figure S30. ^{1}H-NMR spectra of Ce-Cu-CDs-5% in –1.2~–1.7 V (*vs.* RHE).

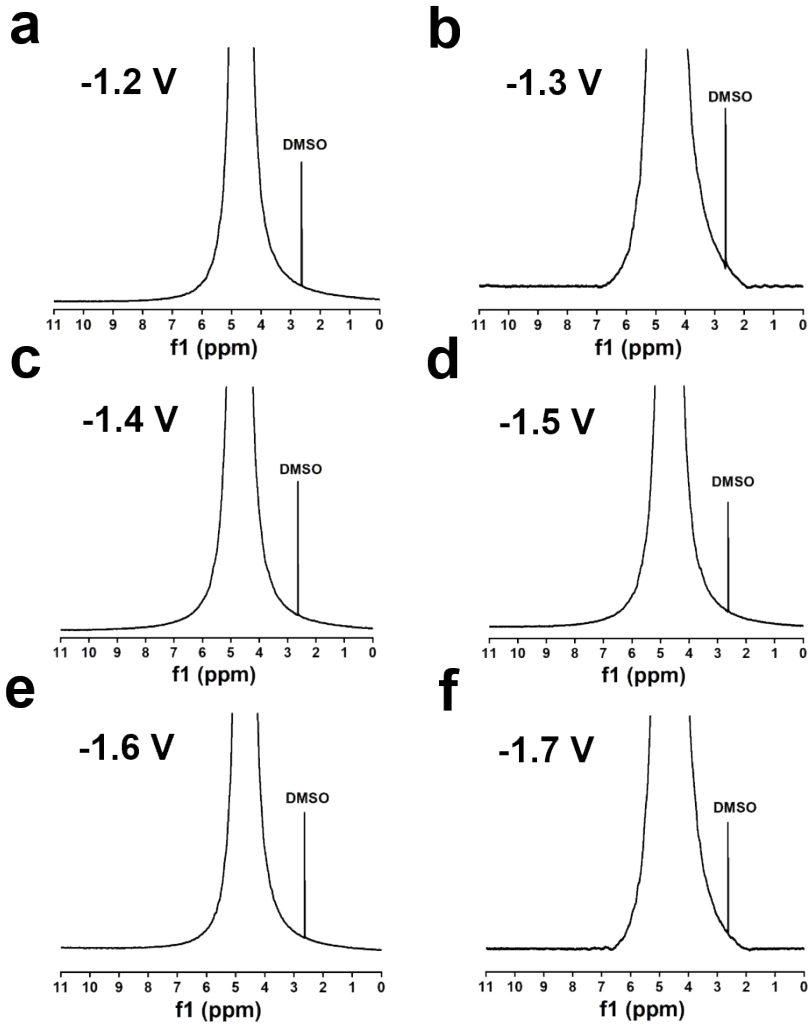

Figure S31. ^{1}H-NMR spectra of CeO_2 in –1.2~–1.7 V (*vs.* RHE).

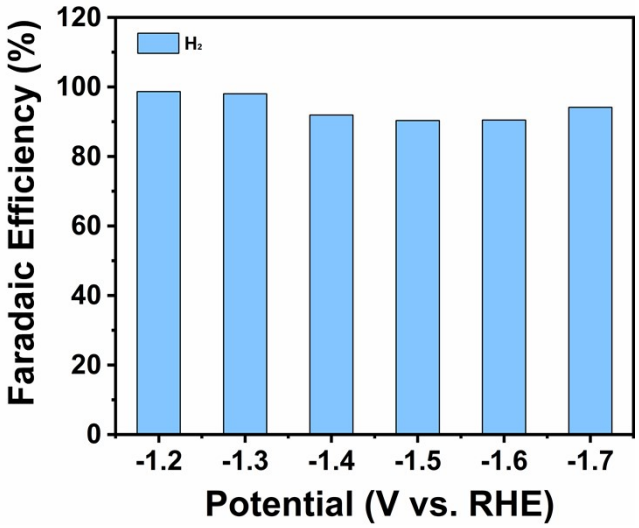

Figure S32. Product distributions and corresponding FEs produced by CeO_2.

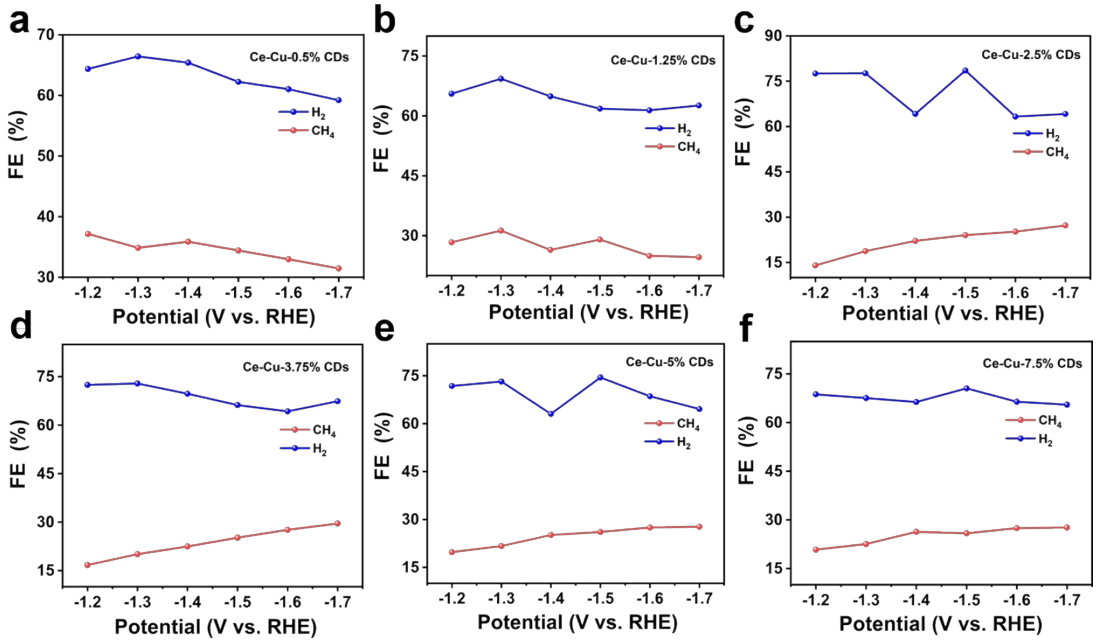

Figure S33. FE of CH_4 and H_2 of Ce-Cu with different concentrations of CDs under different potentials.

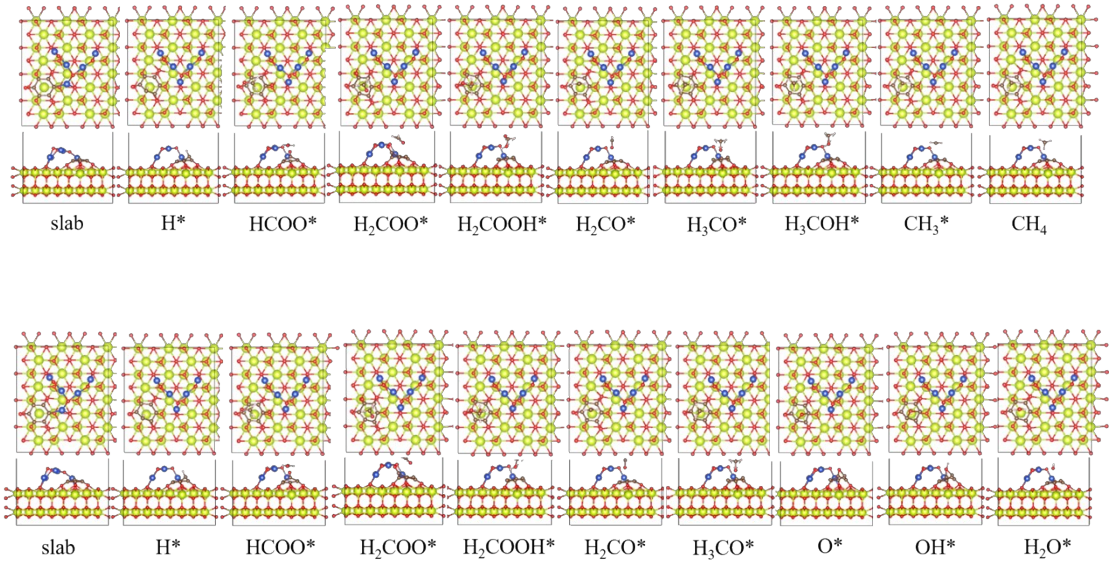

Figure S34. Optimized structures of the reaction intermediates for CO_2 reduction on Ce-Cu-CDs.

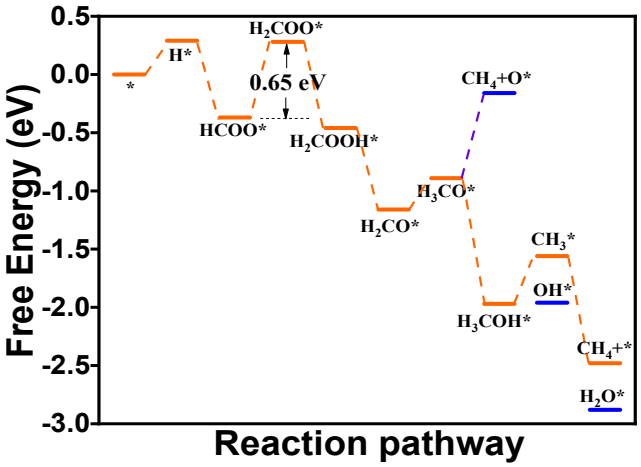

Figure S35. The Gibbs free energy diagrams for the CO_2RR on Ce-Cu at the applied potential. The asterisk (*) represents a surface site for adsorption, and the maximum ΔG of the pathways is highlighted in orange.

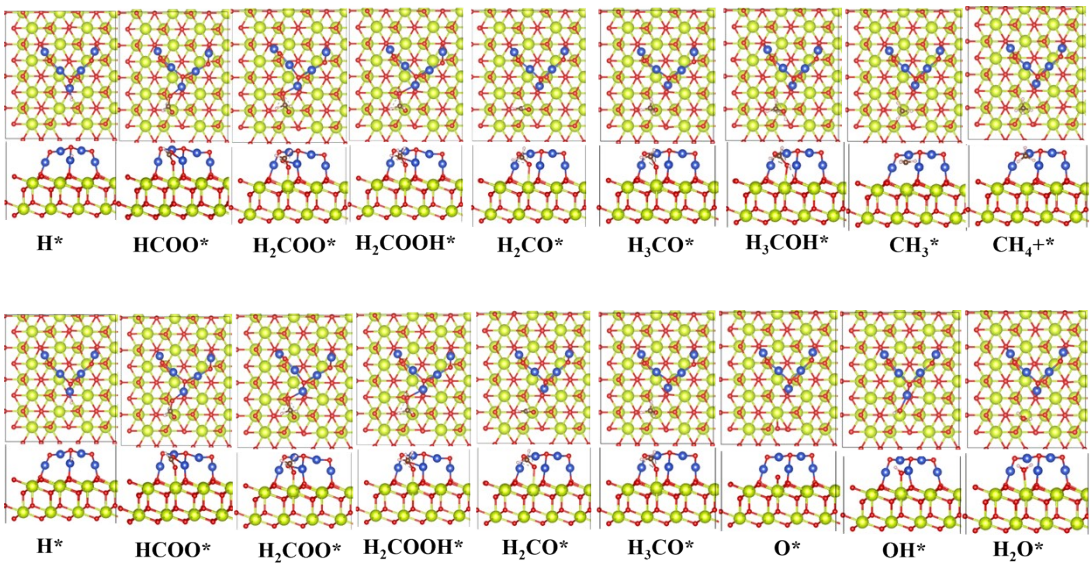

Figure S36. Optimized structures of the reaction intermediates for CO_2 reduction on Ce-Cu.

Table S1. Brunauer–Emmett–Teller (BET) surface areas of CeO_2, Ce-Cu, Ce-Cu-CDs-2.5%.

sample	**BET surface area/$m^2 \cdot g^{-1}$**
CeO_2	77.1
Ce-Cu	52.3
Ce-Cu-CDs-2.5%	26.5

References

1. H. Si, Z. Li, T. Zhang, Z. Fan, H. Huang, Y. Liu and Z. Kang, *Appl. Surf. Sci.*, 2024, **649**, 159153.
2. G. Kresse and J. Furthmüller, *Comput. Mater. Sci.*, 1996, **6**, 15–50.
3. G. Kresse and D. Joubert, *Phys. Rev. B*, 1999, **59**, 1758–1775.
4. J. P. Perdew, K. Burke and M. Ernzerhof, *Phys Rev Lett*, 1996, **77**, 3865–3868.
5. S. Grimme, J. Antony, S. Ehrlich and H. Krieg, *J. Chem. Phys.*, 2010, **132**, 。154104.
6. D. J. Chadi, *Phys Rev B*, 1977, **16**, 1746–1747.